WheatOmics (2026) 2:8
https://doi.org/10.1007/s44412-026-00014-w

RESEARCH

NLR$_{4DS-1}$ enhances wheat resistance to stripe rust by upregulating multiple defense responses

Jicheng Qu[1] · Hongyun Kou[1] · Zhenghan Chen[1] · Muhammmad Waqas[1,2] · Hao Wang[1] · Fengchang Ye[1] · Mingzhu Lyu[1] · Heng Tang[1] · Jiajie Wu[1] · Daolin Fu[1,2]

Received: 6 March 2026 / Revised: 23 May 2026 / Accepted: 25 May 2026
© The Author(s) 2026

Abstract

Key message *NLR*$_{4DS-1}$ confers stripe rust resistance by enhancing multilayer physical and chemical defenses. This finding illuminates strategies for engineering durable resistance in wheat.

Abstract Wheat stripe rust (*Puccinia striiformis* f. sp. *tritici*, *Pst*) is a major threat to global wheat production. The *Yr28* locus for *Pst* resistance is derived from *Aegilops tauschii* subsp. *strangulata*. *NLR*$_{4DS-1}$ has been identified as the stripe rust resistance gene at the *Yr28* locus, which encodes a coiled-coil nucleotide-binding leucine-rich repeat (NLR) protein, however, its molecular mode of action remains largely unknown. Here, we introduced the full-length genomic *NLR*$_{4DS-1}$ into the *Pst* susceptible wheat 'Fielder' by *Agrobacterium*-mediated transformation. Transgenic plants were resistant to *Pst*, with significantly reduced fungal biomass and elevated expression of pathogenesis-related genes. Integrated transcriptomic and metabolomic analysis revealed that *NLR*$_{4DS-1}$ orchestrates a multifaceted defense program involving a burst of reactive oxygen species, chlorophyll reduction, lignin accumulation, and the induction of flavonoid and terpenoid phytoalexins. In vitro, either the flavonoid quercetin or the terpenoid borneol can suppress spore germination and hyphal growth of *Pst*. Notably, *NLR*$_{4DS-1}$ expression did not compromise seedling growth or agronomic performance at the adult stage. Together, these findings identify *NLR*$_{4DS-1}$ as the stripe rust resistance gene for *Yr28* locus, demonstrate its role in activating defensive pathways, and highlight its potential for engineering durable *Pst* resistance through gene stacking.

Keywords Alternative splicing · Phytoalexins · *Puccinia striiformis* · *Triticum aestivum* · *Yr28*

1 Introduction

Wheat stripe rust (yellow rust or *Yr*; *Puccinia striiformis* f. sp. *tritici* or *Pst*) is a major constraint on global wheat production. *Yr* resistance in the host is the best method for *Pst* control, but *Yr* genes are often overcome by the rapid evolution of *Pst* populations (Chen et al. 2014). Consequently, identifying durable *Yr* genes and understanding their molecular mechanisms are necessary; Currently the lack of a clear model for any durable *Yr* genes constrains their application in wheat improvement.

Of the fifteen cloned *Yr* genes, *Yr36* is one of a few with a known mode of action. *Yr36* encodes the kinase WKS1 (Wheat Kinase START1) (Fu et al. 2009). The predominant transcript, WKS1.1, phosphorylates multiple downstream targets, which are involved in redox regulation, photosynthesis, lipid metabolism, carotenoid biosynthesis, and carbohydrate allocation (Gou et al. 2015; Wang et al. 2019; Yan et al. 2023, 2025; Chang et al. 2023). These studies establish that WKS1.1 is a core regulator for multiple metabolic and defense processes, and provide a benchmark for functional dissection of *Yr* genes. In addition, *Yr10*, *Yr15*, *Yr18* and *Yr46* encode for the NAC transcription factor (Ni et al. 2023; Dibley et al. 2024), the kinase WTK1 (Klymiuk et al. 2018), an ABC transporter (Krattinger et al. 2009), and a hexose transporter (Moore et al. 2015), respectively, which are all noncanonical resistance proteins. In contrast, most of the other known *Yr* genes encode for nucleotide-binding

✉ Jiajie Wu
jiajiewu@sdau.edu.cn

✉ Daolin Fu
dlfu@sdau.edu.cn

[1] State Key Laboratory of Wheat Improvement, College of Agronomy, Shandong Agricultural University, Tai'an 271018, China

[2] Spring Valley Agriscience Co., Ltd, Jinan 250300, China

Published online: 19 June 2026

leucine-rich repeat (NLR) proteins, including *Yr5*, *Yr6*, *Yr7*, *Yr9*, *Yr28*, *Yr84*, *Yr87*, *YrSP*, *YrU1*, and *YrTD121* (Lyu et al. 2025; Wang et al. 2020; Hu et al. 2025). For example, the *Yr28* (or *YrAS2388*) locus harbors the NLR gene NLR_{4DS-1}, which produces multiple transcript variants (*TV1-TV4*), among which the full-length transcript *TV1* encodes a typical coiled-coil (CC), nucleotide-binding (NB) and leucine-rich repeat (LRR) protein (Zhang et al. 2019). Despite extensive cloning efforts, the downstream defensive pathways activated by most *Yr* proteins, particularly NLR-type genes, remain largely unknown.

Plant immunity is mediated by pathogen-associated molecular pattern (PAMP)-triggered immunity (PTI) and effector-triggered immunity (ETI) (Jones and Dangl 2006; Ngou et al. 2022). Although PTI and ETI are initiated by distinct recognition events, they converge on shared downstream defense mechanisms. Upon pathogen recognition, plants activate a suite of defense responses, including reactive oxygen species (ROS) production, hormone signaling, programmed cell death (PCD), cell wall reinforcement, and secondary metabolite biosynthesis (Ishihama et al. 2021; Ngou et al. 2022; Ortiz-Morea et al. 2022). ROS not only exert direct antimicrobial activity but also function as signaling molecules that amplify downstream defense responses (Yang et al. 2022). For biotrophic pathogens, the ROS burst is associated with chlorophyll degradation and reduced photosynthesis, thereby constraining pathogen growth by limiting nutrients availability; in contrast, localized leaf regions that retain normal chlorophyll content can form 'green islands', which may provide a favorable environment for the pathogen (Walters et al. 2008; Naseem et al. 2014). In parallel, plant immunity also relies on structural reinforcement and metabolic reprogramming. Lignin deposition enhances secondary cell wall strength and impedes pathogen penetration (Lee et al. 2019); enhanced lignin biosynthesis can confer broad-spectrum resistance in crops such as rice and wheat (He et al. 2023; Li et al. 2020). Secondary metabolites, particularly flavonoids and terpenoids, constitute another important defense layer, acting either as antimicrobial compounds or as immune signals. Examples include monoterpene-mediated resistance in Norway spruce (Wang et al. 2025a), kinase-regulated diterpenoid biosynthesis in rice (Wang et al. 2023), and flavonoid accumulation associated with early-stage *Pst* resistance in wheat (Kong et al. 2025). Collectively, coordinated regulation of redox signaling, metabolic defense, and cell wall fortification underpins effective plant immune responses.

The *Yr28* locus, which was introgressed from *Aegilops tauschii*, was proposed to be NLR_{4DS-1} (Zhang et al. 2019); however, the function of NLR_{4DS-1} and its downstream defense pathways remain largely unresolved. By integrating transgenic validation with transcriptomic and metabolomic profiling, we prove that NLR_{4DS-1} is a central regulator of multi-pathway immunity; this offers a framework for engineering durable *Pst* resistance in wheat.

2 Materials and methods

2.1 Plant materials and growing conditions

The common wheat 'Fielder' control and its transgenic plants with a full-length genomic NLR_{4DS-1} (11,360 bp; Supplementary Fig. 1) were used as experimental materials. Seedling agronomic traits were evaluated 14 days after germination in Hoagland's nutrient solution. Field phenotyping was performed in an outdoor facility at the Daizong Campus of Shandong Agricultural University (Longitude: 117.117673°E, Latitude: 36.19451°N).

2.2 Stripe rust inoculation and disease assessment

Urediniospores of *Pst* race CYR32 were heat-activated at 42 °C for 5 min and then mixed with a tenfold volume of inactivated pine spores or talcum powder. The spore mixture was evenly brushed onto the leaf surfaces using a soft brush. After inoculation, plants were kept in complete darkness for 24 h and subsequently transferred to a growth chamber under a 16 h light (14 °C) / 8 h dark (12 °C) photoperiod. High humidity was maintained by misting the plants with water twice daily. Disease response was assessed using the 0–9 disease scoring scale (McNeal 1971; Hovmøller et al. 2017) at 10, 11, and 12 days post inoculation (dpi).

2.3 RNA extraction, library preparation, and sequencing

To perform RNA-seq, leaf samples of WT and transgenic plants were collected at 0 and 24 h post inoculation (hpi) with three biological replicates. Total RNA was extracted using TRIzol reagent (TIANGEN, DP424). Sequencing libraries were constructed by following instructions of the KC™ mRNA Library Prep Kit (Wuhan Kangce Biotechnology). During library preparation, PCR products between 200 and 500 bp were enriched and sequenced on the DNBSEQ-T7 platform (MGI Tech) using a PE150 (paired-end 150 bp) sequencing strategy.

2.4 RNA-seq data and analysis

Raw sequencing data were processed using fastp (version 0.23.0) for quality control. Clean reads were mapped to the Fielder genome (https://shigen.nig.ac.jp/wheat/komugi/genome/download.jsp). Gene expression was quantified using

Transcripts Per Million (TPM) values (Zhao et al. 2020). Differentially expressed genes (DEGs) were identified using the DEGseq R package, with significance thresholds set at $|\log_2 FC| > 1$ and an adjusted p-value < 0.05. Functional annotation of DEG-encoded proteins was performed using TBtools, including: Gene Ontology (GO) annotation and enrichment analysis and Kyoto Encyclopedia of Genes and Genomes (KEGG) pathway annotation and enrichment analysis.

Expression values (transcripts per kilobase million or TPM for transcriptome data) in each sample were normalized using the Min-Max scaling method. This technique linearly scales expression values to a specified range between minimum and maximum values. Specifically, for each sample, the expression value was (1) subtracted by the sample's minimum value; (2) divided by the difference between the sample's maximum and minimum values; and (3) resulting in data constrained to the [0, 1] range. The normalized data were then visualized as heatmaps using GraphPad Prism 8. Bar graphs represent mean ± s.e.m. Statistical significance was determined by two-tailed t-test, exemplified as ns (not significant, $P > 0.05$), * ($0.01 < P \leq 0.05$), ** ($0.001 < P \leq 0.01$), *** ($0.0001 < P \leq 0.001$) and **** ($P \leq 0.0001$).

2.5 Quantitative PCR analysis

Total RNA was treated with DNaseI and reverse transcribed using the HiScript III RT SuperMix (Vazyme Biotech, R433). The cDNA products were used for quantitative RT-PCR (qRT-PCR) according to the manufacturer's instructions for the ChamQ Universal SYBR qPCR Master Mix (Vazyme Biotech, Q312). qRT-PCR reactions were performed on a StepOnePlus™ Real-Time PCR System (Applied Biosystems™, Thermo Fisher Scientific). Gene expression was determined by the $2^{-\Delta\Delta CT}$ method (Schmittgen and Livak 2008).

2.6 3,3′-diaminobenzidine staining

After the CYR32 inoculation, wheat leaves were collected at 0, 24, 48, 96, and 144 hpi. Leaf segments were vacuum-infiltrated with a 1% (w/v) 3,3'-diaminobenzidine (DAB) aqueous solution and stained for 24 h at room temperature. After staining, leaves were rinsed 3–5 times with distilled water, wiped with filter paper, and destained in 95% ethanol until a complete loss of chlorophyll. Hydrogen peroxide reaction was visualized and documented using a brightfield microscope (Olympus).

2.7 Staining and quantification of lignin

Histochemical staining: CYR32-infected leaves were sampled at 96 hpi. Samples were soaked in acetic acid: ethanol (1:3, v/v) until a complete loss of chlorophyll, rinsed for 10 h in distilled water, wiped with filter paper, and then stained in 1% phloroglucinol (w/v in 50% HCl) for 5 h. Lignin deposition was visualized and documented using a stereomicroscope (Olympus).

Lignin quantification: Leaf samples (1 g) were collected at 96 hpi, dried at 42 °C, and acetylated by following the Lignin Content Assay Kit (Solarbio, BC4200). The absorbance of the solution was measured using a spectrophotometer (Thermo Fisher Scientific). Lignin concentration was calculated using the formula: Lignin content (mg/g)=(ΔA×V_assay)/(ε × d×V_supernatant × W/V_acetylation) = 2.184 × ΔA/W(ΔA: Absorbance difference at characteristic wavelength; ε: Molar extinction coefficient of lignin (23.35 $mL \cdot mg^{-1} \cdot cm^{-1}$); d: Light path length (1 cm); V_assay: Assay volume (1 mL); V_supernatant: Supernatant volume (0.02 mL); V_acetylation: Acetylation reaction volume (1.02 mL); W: Sample dry weight (g) (Janshekar et al. 1981).

2.8 Quantification of chlorophyll content

At 5 dpi with CYR32, wheat leaves (1 g) were homogenized in 10 mL 95% ethanol. After filtration, the homogenate was adjusted to 50 mL by supplying 95% ethanol. Absorbance of the chlorophyll extract was measured at 665 nm and 645 nm using 95% ethanol as a blank control (Mamrutha et al. 2017). Chlorophyll content was calculated according to Arnon's equations: chlorophyll a (μg/mL) = (13.95 × A_{665}) - (6.80 × A_{645}); chlorophyll b (μg/mL) = (24.96 × A_{645}) - (7.32 × A_{665}) (Wang et al. 2011).

2.9 Liquid chromatography-mass spectrometry and data analysis

Metabolomics were based on the ACQUITY UPLC I-Class Plus ultra-high-performance liquid chromatography system coupled with a Q Exactive™ Plus high-resolution mass spectrometer (LC-MS/MS). Separation was performed on an ACQUITY UPLC HSS T3 column (1.8 μm, 2.1 × 100 mm) under both positive and negative ionization modes. Raw LC-MS data were processed using Progenesis QI software (v2.3, Nonlinear Dynamics, Newcastle, UK). Compound identification was based on the Human Metabolome Database (HMDB), LIPID MAPS (v2.3), METLIN, and an in-house database (based on: Precise mass-to-charge ratio (m/z); secondary fragmentation patterns; isotopic distributions). Variable Importance in Projection (VIP) values

derived from Orthogonal Projections to Latent Structures-Discriminant Analysis (OPLS-DA) models ranked the contribution of each variable to group discrimination. Statistical significance of inter-group metabolite differences was assessed using two-tailed Student's t-tests. Differentially accumulated metabolites were selected with VIP > 1.0 and p-value < 0.05.

2.10 In vitro antimicrobial activity assay of quercetin and borneol against *Pst*

To assess the anti-*Pst* activity of differential metabolites, fresh *Pst* urediniospores were incubated with quercetin and borneol solutions, using water as control, and incubated at room temperature for 24 h. Spore germination and hyphal growth were observed under an optical microscope.

Seedlings of wild-type Fielder were inoculated with CYR32, and were sprayed with water as control, 100 μM quercetin (Aladdin, Q111273, purity ≥ 98.5%) or 100 μM borneol (Macklin, B794507, purity ≥ 99.0%). *Pst* infection was evaluated at 14 dpi.

2.11 Subcellular Localization of $NLR_{4DS\text{-}1}$

Each of the four $NLR_{4DS\text{-}1}$ transcript variants was cloned into a vector driven by the CaMV 35 S (35 S) promoter, with a GFP tag fused in-frame at the 3′ end. The resulting constructs were transformed into Agrobacterium tumefaciens strain EHA105 and subsequently infiltrated into tobacco leaves. After 2–3 days, subcellular localization was observed under a fluorescence microscope (LSM 880 NLO, Zeiss). The excitation and detection wavelengths were approximately 488 nm and 509 nm for GFP, and approximately 587 nm and 610 nm for mCherry, respectively.

3 Result

3.1 NLR_{4DS-1} transgene confers stripe rust resistance in wheat

A full-length genomic allele of NLR_{4DS-1} (11,360 bp), from *Ae. tauschii* accession 'PI511383', was introduced into common wheat Fielder, which resulted in 21 independent transgenic lines. Fifteen of the T_0 plants were resistant to CYR32. The T_1 lines PC1334-1, -15, -16, -18, and -27, which were positive for the NLR_{4DS-1} transgene both in integration and transcription (Fig. 1a), were used for further studies.

With CYR32 infection, the NLR_{4DS-1} plants had lower infection types (ITs 0–5) than those in the wild-type (WT) Fielder (ITs 7–9) (Supplementary Table 1). At 12 dpi,

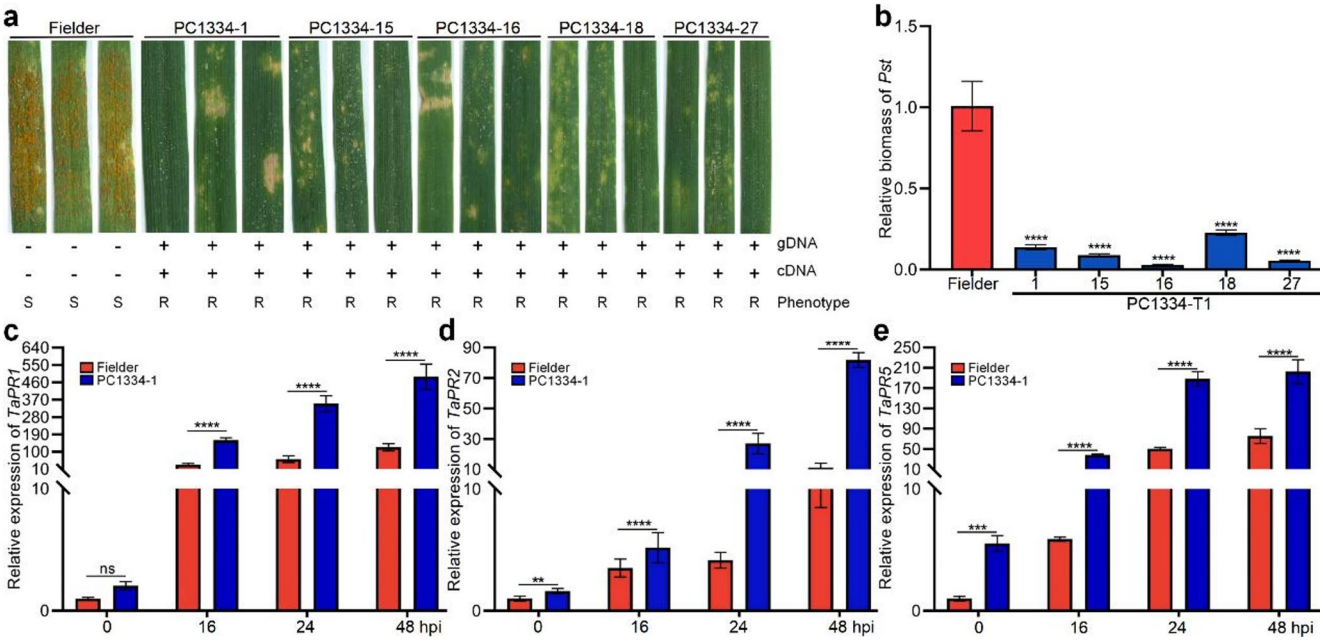


Fig. 1 Transgene NLR_{4DS-1} confers *Pst* resistance and activates *PR* gene expression in wheat. **a**, Phenotypes of the T_1 lines and the WT Fielder control at 12 dpi with CYR32. The integration and transcription of NLR_{4DS-1}, either positive ('+') or negative ('–'), were determined with genomic DNA (gDNA) and complementary DNA (cDNA), respectively. Disease responses were scored as either resistant (R) or susceptible (S). **b**, Relative *Pst* biomass in CYR32-infected leaves was quantified by qRT-PCR using relative quantities of *PstEF1α* and *TaEF1α*. **c**–**e**, Quantitative expression of pathogenesis-related (PR) genes *TaPR1* (*TraesFLD7D01G187700*), *TaPR2* (*TraesFLD3B01G594800*), and *TaPR5* (*TraesFLD5A01G020900*) in the WT Fielder and transgenic T_1 plants at 0, 16, 24, and 32 hpi. *TaEF1α* is an internal gene control in wheat. Error bar represents ± standard error of the mean (s.e.m.)

NLR_{4DS-1} plants were resistant with only localized necrotic lesions and few pustules, whereas extensive sporulation occurred in WT Fielder (Fig. 1a). Within leaves, NLR_{4DS-1} plants also had less CYR32 biomass than the Fielder control (Fig. 1b). As a result, CYR32 infection upregulated pathogenesis-related (PR) genes, such as *TaPR1*, *TaPR2*, and *TaPR5* in PC1334-1 (Fig. 1c-e). Thus, NLR_{4DS-1} alone is sufficient to activate multiple resistance pathways for stripe rust.

3.2 NLR_{4DS-1} drives transcriptome reprogramming upon *Pst* infection

To study NLR_{4DS-1}-specific defense pathways, we conducted mRNA sequencing in the WT Fielder and the NLR_{4DS-1} plants (PC1334-1, $n=3$) at 0 and 24 hpi with *Pst* (CYR32). In total, 970,510,328 clean and high-quality reads (~143.55 Gb) were obtained, for which Q30 values were >98.10%, GC content ranged from 55.48% to 57.58%, and the mapping rates were >96.95% (Supplementary Table 2).

A total of 3,798 differentially expressed genes (DEGs) were identified between PC1334-1 and Fielder. 64.51% of the DEGs (2,450) were detected at 24 hpi; in comparison to 22.43% of the DEGs (852) at 0 hpi, 13.01% of the DEGs (496) were conserved between 0 and 24 hpi (Supplementary Fig. 2a, b). At 24 hpi, 2,323 DEGs were upregulated, and 623 were downregulated; *Pst* infection enhanced the NLR_{4DS-1}-specific transcriptomes. qRT-PCR also validated the RNA-seq result ($R^2 = 0.8489$; Supplementary Fig. 3).

Both GO and KEGG analyses revealed a functional divergence at 24 hpi. Upregulated DEGs were uniquely enriched in 280 GO terms and 54 KEGG pathways at 24 hpi, whereas downregulated DEGs were associated with 124 GO terms and 30 KEGG pathways (Supplementary Fig. 2c-f). Thus, *Pst* infection induces NLR_{4DS-1}-driven transcriptome reprogramming.

3.3 NLR_{4DS-1} causes more ROS, and less chlorophyll and senescence at the *Pst* infection site

Among GO terms of the NLR_{4DS-1}-upregulated DEGs at 24 hpi, ten are ROS-related (Fig. 2a). In the RNA-seq data, many ROS-related genes were upregulated in the NLR_{4DS-1} plant than the ones in Fielder at 24 hpi (Supplementary Fig. 4a). The induction of four genes in NLR_{4DS-1} plants wereas validated by qRT-PCR (Fig. 2b-e). Importantly, more ROS accumulated at the *Pst*-infection sites in the NLR_{4DS-1} plants than in the WT Fielder at 24, 48, 96, and 144 hpi (Fig. 2f).

In contrast, the NLR_{4DS-1}-downregulated GO terms at 24 hpi were predominantly related to chlorophyll metabolism and chloroplast function (Fig. 3a); this was further supported by the KEGG enrichment of photosynthesis-related pathways (Supplementary Fig. 5a). In *Pst*-infected plants with NLR_{4DS-1}, many genes for chlorophyll biosynthesis and photosynthesis were suppressed (Supplementary Fig. 4b); this result was validated by qRT-PCR (Fig. 3b-e). Thus, whereas the chlorophyll a and b contents were comparable between the NLR_{4DS-1} plants and Fielder at 0 dpi (Fig. 3f), at 5 dpi, the NLR_{4DS-1} plants had significantly less chlorophyll a and b than Fielder (Fig. 3g).

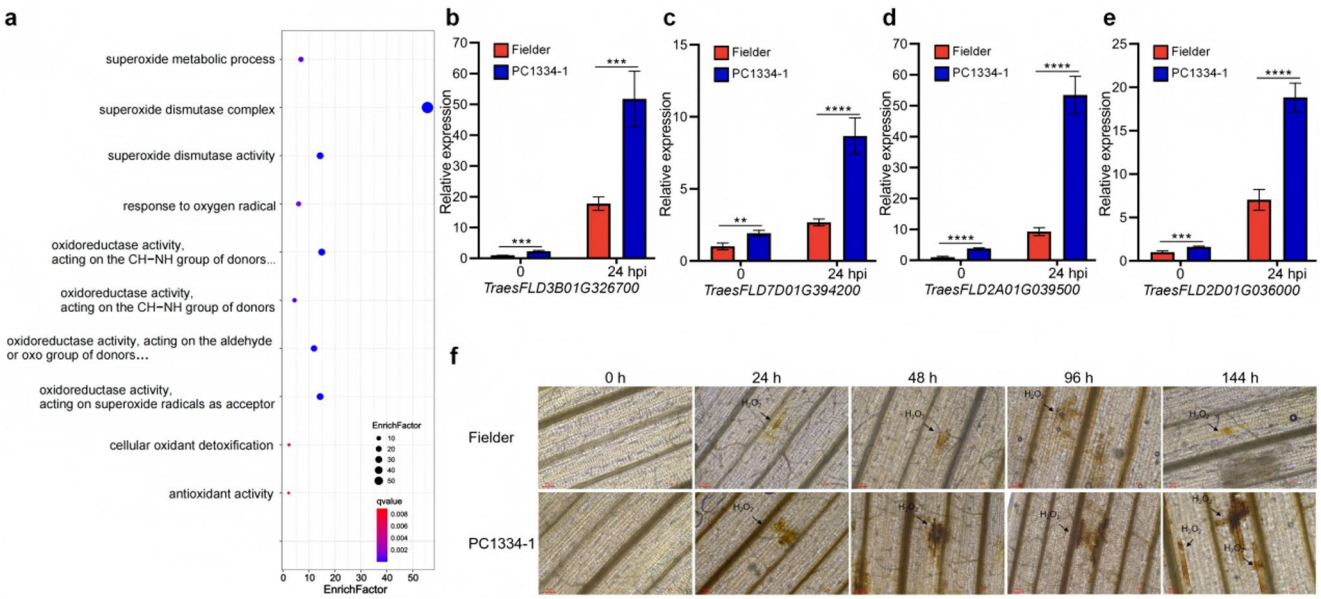


Fig. 2 NLR_{4DS-1} indirectly activates ROS production and signaling during wheat-*Pst* interaction. **a**, ROS-related GO terms from the NLR_{4DS-1} plant (PC1334-1) at 24 hpi. **b–e**, Transcription of four ROS-related genes as revealed by qRT-PCR. **f**, DAB staining of ROS (10× magnification)

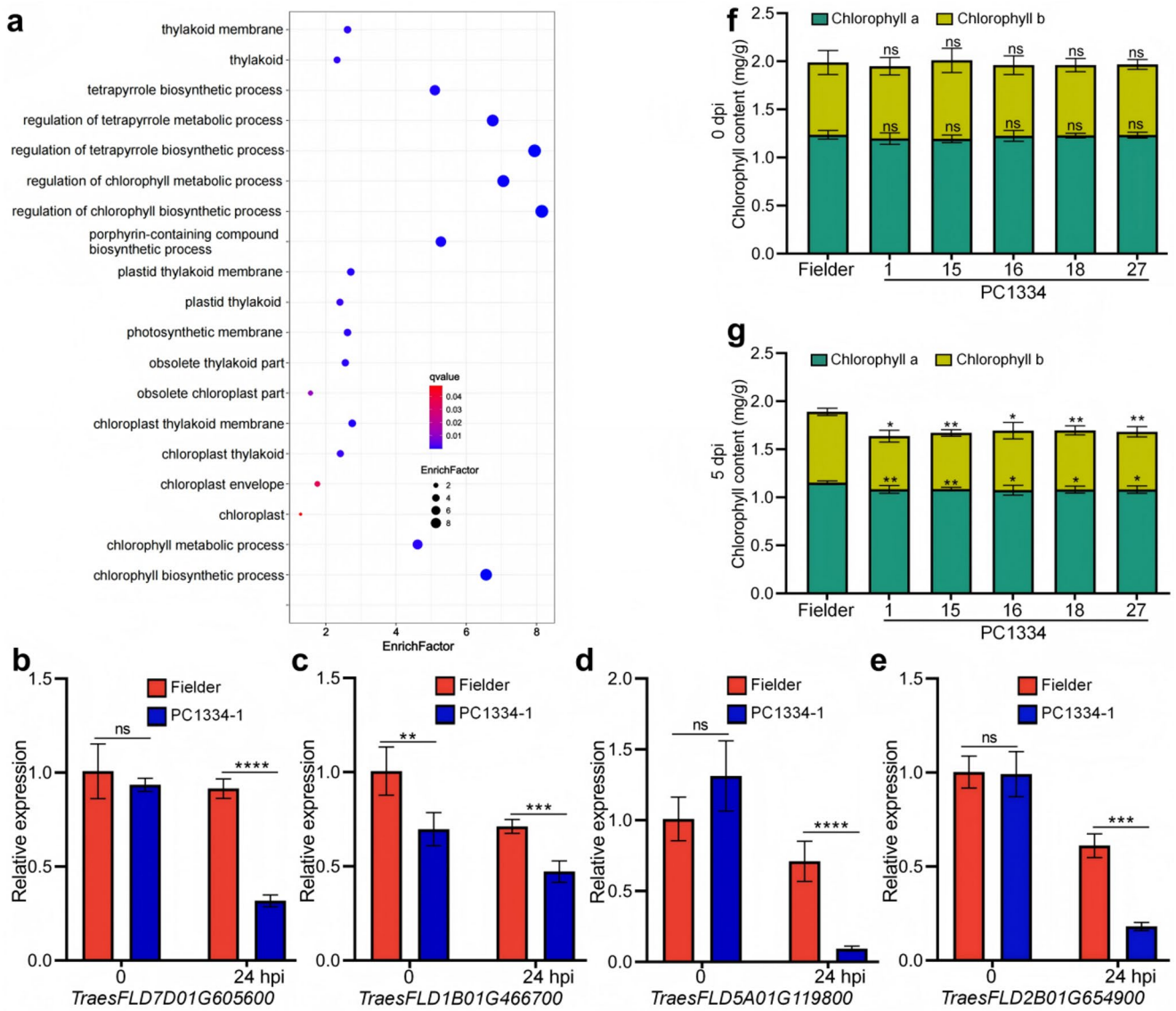


Fig. 3 NLR_{4DS-1} suppresses photosynthesis and chlorophyll metabolism during the wheat-*Pst* interaction. **a**, Photosynthesis- and chlorophyll-related GO terms from the NLR_{4DS-1} plant (PC1334-1) at 24 hpi. **b–e**, Transcription of 4 photosynthesis-related genes as revealed by qRT-PCR. **f**, Chlorophyll content (a and b) in the NLR_{4DS-1} transgenic (PC1334-1) and Fielder at 0 dpi. **g**, Chlorophyll content (a and b) in the NLR_{4DS-1} transgenic (PC1334-1) and Fielder at 5 dpi

Approximately 12 days post the CYR32 inoculation, the NLR_{4DS-1} plants developed chlorotic or necrotic lesions at the infection sites (Fig. 1a), which is a sign of tissue senescence. In fact, multiple senescence-associated genes (SAGs), including *TraesFLD4B01G081000*, *TraesFLD5B01G128000*, *TraesFLD5D01G140100*, *TraesFLD5A01G059800*, *TraesFLD5B01G068700* and *TraesFLD5D01G074400*, were significantly upregulated in the NLR_{4DS-1} plants (PC1334-1) than those in the WT Fielder at 24 hpi (Supplementary Fig. 6a-f). Thus, at the infection site, NLR_{4DS-1} causes ROS accumulation and chlorophyll reduction, and upregulation of genes associated with tissue senescence.

3.4 NLR_{4DS-1} enhances lignin biosynthesis and accumulation

7 GO terms associated with lignin biosynthesis were enriched in the NLR_{4DS-1} plant (PC1334-1) at 24 hpi (Fig. 4a). Upregulation of the lignin biosynthesis genes (Supplementary Fig. 4c) was partially confirmed by specific qRT-PCR of selected genes (Fig. 4b-e). Lignin content was comparable between the NLR_{4DS-1} and Fielder plants at 0 hpi, but lignin content was significantly higher in NLR_{4DS-1} plants than in WT Fielder at 96 hpi (Fig. 4f-g). Thus, after *Pst* infection in a resistant interaction, NLR_{4DS-1} upregulates

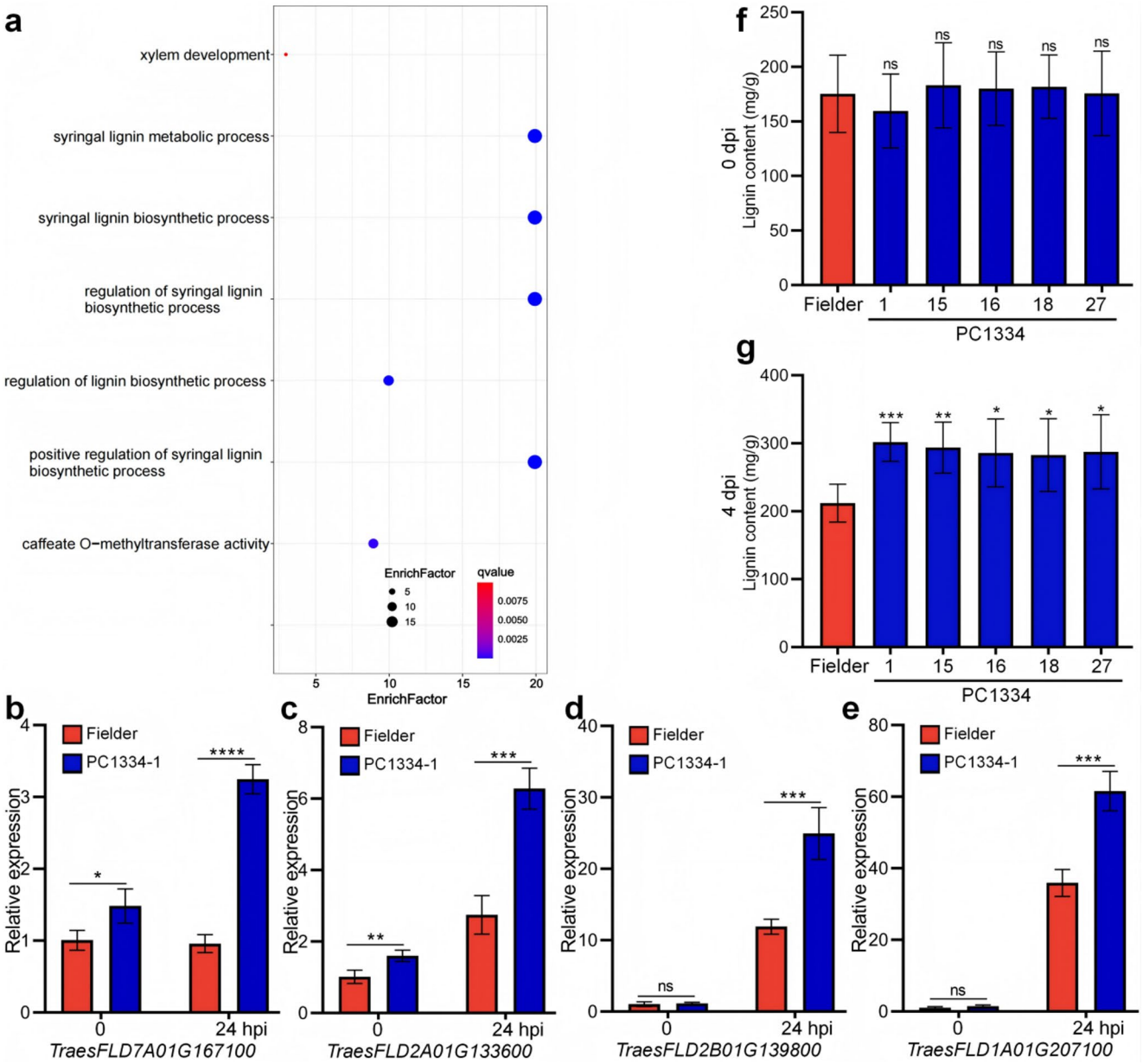


Fig. 4 NLR_{4DS-1} activates lignin biosynthesis during wheat-*Pst* interaction. **a**, Lignin-related GO terms. **b-e**, Transcription of lignin biosynthesis genes as revealed by qRT-PCR. **f-g**, Lignin content in leaves of 5 T_1NLR_{4DS-1} lines (PC1334 -1, -15, -16, -18 and −27) and WT Fielder at 0 (**f**) and 96 hpi (**g**). Statistical significance was determined by two-tailed *t*-test

lignin biosynthesis, which presumably enhances cell wall-based defense.

3.5 NLR_{4DS-1} activates flavonoid and terpenoid biosynthesis during *Pst* infection

Metabolomic profiling was performed to understand the NLR_{4DS-1}-mediated *Pst* resistance. In total, there were 1,237 differentially accumulated metabolites (DAMs) in the NLR_{4DS-1} plants when compared to the Fielder control, of which 654 DAMs were specific at 0 hpi, 397 at 24 hpi, and 186 at both 0 and 24 hpi (Supplementary Fig. 7a). Notably, NLR_{4DS-1} upregulated 273 and 324 metabolites at 0 and 24 hpi, respectively, but downregulated 567 and 259 metabolites at 0 and 24 hpi, respectively (Supplementary Fig. 7b). Thus, when *Pst* infects, NLR_{4DS-1} causes broad-spectrum metabolic reprogramming.

Of the 259 NLR_{4DS-1}-specific DAMs at 24 hpi, some flavonoids were differentially accumulated, including 4'-O-methyldavidioside, broussinol, catechin 5-O-beta-D-apiofuranoside, kaempferol 3-(2''-p-coumaryl-alpha-L-arabinopyranoside), leucodelphinidin, quercetin

3-galacturonide, SCHEMBL15543426, sigmoidin G, topazolin hydrate, and trans-anhydrotephrostachin (Fig. 5b). Similarly, GO and KEGG analyses indicated an enrichment in the flavonoid biosynthetic pathways in the NLR_{4DS-1} plants at 24 hpi (Fig. 5a, Supplementary Fig. 5b). The NLR_{4DS-1}-specific upregulation of flavonoid biosynthesis genes (Supplementary Fig. 4d) was partially confirmed by qRT-PCR (Supplementary Fig. 8a-e).

Coincidentally, in *Pst*-infected transgenic NLR_{4DS-1} plants (PC1334-1), terpenoid biosynthesis was markedly induced. At 24 hpi, 12 terpenoid-related GO terms were enriched among upregulated DEGs (Fig. 5c), and monoterpenoid biosynthesis was the most significantly enriched

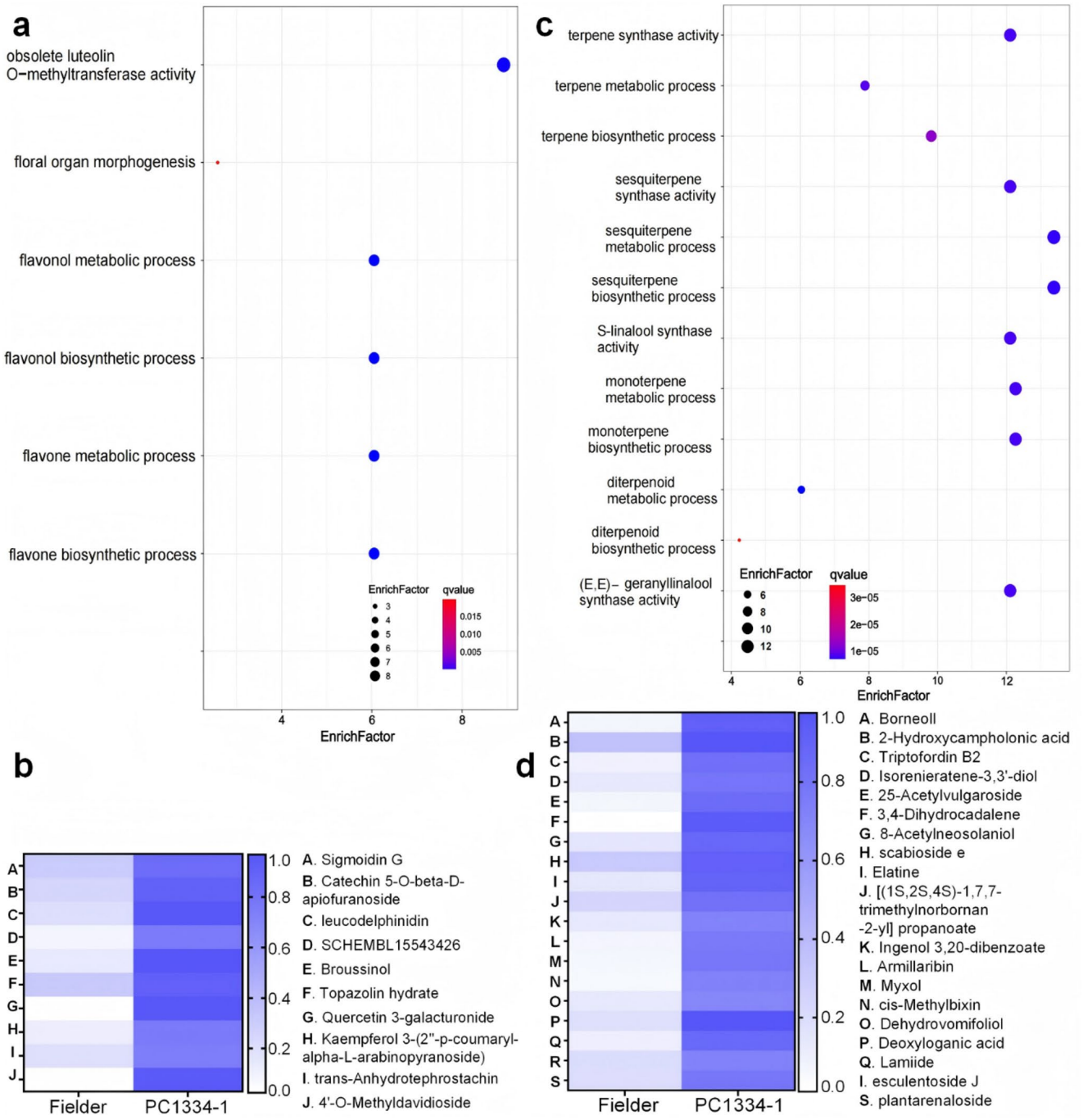


Fig. 5 NLR_{4DS-1} activates flavonoid and terpenoid biosynthesis upon *Pst* infection. **a**, Enrichment of the flavonoid-related GO terms in NLR_{4DS-1}-upregulated DEGs at 24 hpi. **b**, Heatmap of differentially accumulated flavonoid metabolites. **c**, Enrichment of terpenoid-related GO terms. **d**, Heatmap of differentially accumulated terpenoid metabolites. Metabolite abundance was normalized using the max–min method ($n=3$) (Vafaei et al. 2022)

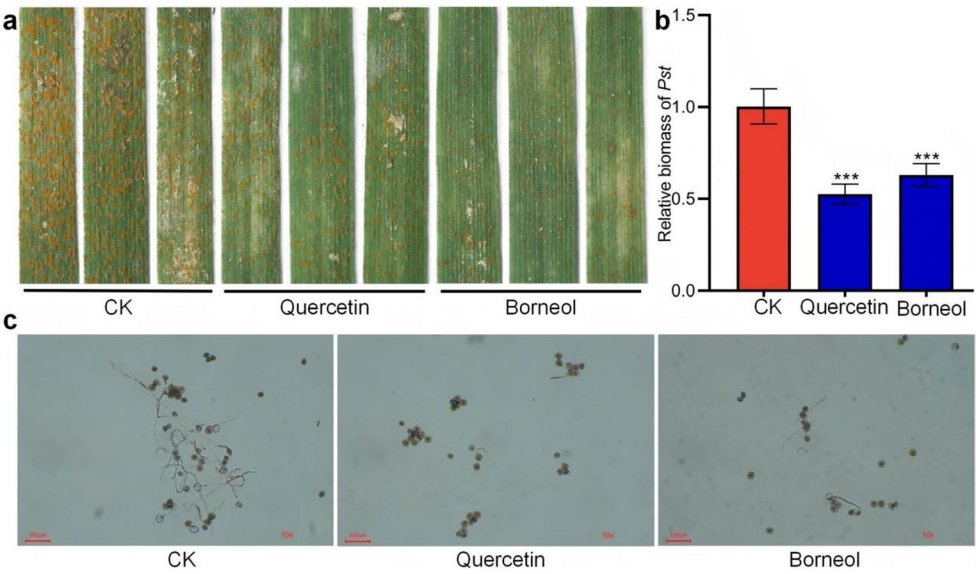


Fig. 6 The effect of a selected flavonoid or terpenoid on *Pst* growth. a, Two-week-old Fielder seedlings were inoculated with CYR32. Experimental groups were foliar-sprayed with either 100 µM quercetin, 100 µM borneol, or 1% (v/v) DMSO in water controls (CK). Leaf phenotypes were recorded at 12 dpi. b, *Pst* biomass in inoculated leaves was quantified by qRT-PCR. c, CYR32 urediniospores were incubated for 24 h in water, 100 µM quercetin, or 100 µM borneol solutions. Spore germination and hyphal growth were observed under 10× magnification

KEGG pathway (Supplementary Fig. 5b). The upregulation of terpenoid biosynthetic genes was confirmed by qRT-PCR (Supplementary Fig. 8e-h). Consistent with these transcriptomic signatures, metabolomic analysis also identified 19 NLR_{4DS-1}-specific terpenoids, including [(1 S,2 S,4 S)-1,7,7-trimethylnorbornan-2-yl] propanoate, 25-acetylvulgaroside, 2-hydroxycampholonic acid, 3,4-dihydrocadalene, 8-acetylneosolaniol, armillaribin, borneol, cis-methylbixin, dehydrovomifoliol, deoxyloganic acid, elatine, esculentoside J, ingenol 3,20-dibenzoate, isorenieratene-3, lamiide, myxol, plantarenaloside, scabioside E, and triptofordin B2 (Fig. 5d). Thus, NLR_{4DS-1} activates flavonoid and terpenoid biosynthesis, which apparently contributes to a broad-spectrum metabolic defense response against *Pst*.

The *Pst*-infected WT Fielder were treated with the flavonoid quercetin or the terpenoid borneol to test their efficacy towards *Pst* resistance. Both quercetin and borneol suppressed the density and biomass of *Pst* than water controls (Fig. 6a, b). In vitro, *Pst* spores exhibited impaired germination and hyphal growth when cultured in aqueous solutions with quercetin or borneol, but appeared normal in water controls (Fig. 6c). Thus, quercetin and borneol can directly suppress *Pst* development, mediating the NLR_{4DS-1}-based *Pst* resistance.

4 Discussion

4.1 NLR_{4DS-1} with multiple transcript isoforms confers *Pst* resistance in wheat

Here we show that NLR_{4DS-1}, driven by its native promoter from *Ae. tauschii*, is sufficient to confer excellent resistance to *Pst* in wheat. The NLR_{4DS-1} gene, one of the functional genes in the 39-kb region, is the stripe rust resistance gene at the *Yr28* locus (Zhang et al. 2019). Previously, only the cDNA sequences of the TV1 and TV2 transcripts, which are specific to the first 3′UTR of NLR_{4DS-1}, were transformed into wheat (Zhang et al. 2019), and neither conferred *Pst* resistance. Athiyannan et al. (2022) later showed that transgenic wheat expressing NLR_{4DS-1} with only the first 3′UTR exhibited weak resistance to *Pst*. In the present study, transformation with the full-length genomic sequence of NLR_{4DS-1}, which contains duplicated 3′UTRs (3′UTR1 and 3′UTR2; Supplementary Fig. 1a), conferred robust resistance, further confirming that the complete gene structure is necessary for full function. Based on the distinct expression patterns of the four transcript isoforms, it is also plausible that these isoforms are not functionally equivalent and that a complex interaction among them may be required for effective *Pst* resistance. Subcellular localization analysis showed that all four protein isoforms of NLR_{4DS-1} localize to the plasma membrane, cytoplasm, and ER membrane without obvious differences (Supplementary Fig. 9), indicating that they share overlapping subcellular compartments and likely cooperate in signal perception and immune execution.

Many NLR proteins couple with other NLRs for disease resistance; examples include: *RPS4*/*RRS1* (Huh et al. 2017) and *CHS3*/*CSA1* (Yang et al. 2024) in *Arabidopsis*; *RGA4*/*RGA5* (Cesari et al. 2013), *Pik1*/*Pik2* (Takagi et al. 2013), *PigmR*/*PigmS* (Deng et al. 2017) in rice, and *RXL*/*Pm5e* (Guo et al. 2025), *TdNLR1* and *TdNLR2* (Hu et al. 2025) and *TdCNL1*/*TdCNL5* (Zhu et al. 2025) in wheat. These protein partners collectively implement effector recognition and downstream signaling. NLRs can be divided into sensor NLRs, which perceive pathogen-derived signals, and helper NLRs, which oligomerize to execute immune responses after activation (Wang et al. 2025b; Contreras

et al. 2023). For example, perception of ADPr-ATP by the EDS1–SAG101 complex leads to activation of the helper NLR NRG1A, thereby triggering ETI signaling (Huang et al. 2025; Xiao et al. 2025). Whether NLR_{4DS-1} requires a partner NLR in common wheat and its D-genome progenitor remains unknown. It is possible that the distinct NLR_{4DS-1} isoforms function as sensor and helper among themselves; whether this occurs can be answered in the future.

4.2 NLR_{4DS-1} likely causes multilayered defense responses

NLR proteins are core receptors in effector-triggered immunity (ETI) (Yuan et al. 2021). After *Pst* infected, NLR_{4DS-1} transgenic wheat was associated with nutrient deprivation of *Pst*, structural enforcement and defense chemical accumulation upon *Pst* infection, which formed a multilayered immune strategy. Therefore, NLR_{4DS-1} can motivate many defense pathways during the wheat-*Pst* interaction. ROS have antimicrobial effects and are defensive signaling molecules (Wang et al. 2022; Kong et al. 2024; Wu et al. 2023). For example, ROS induces lignification (Denness et al. 2011; Qian et al. 2023; Zhang et al. 2025). In this study, the NLR_{4DS-1} transgenic wheat showed ROS burst at 24, 48, 96, and 144 hpi, and lignin deposition at 4 dpi. The lignin deposition then reinforces the cell wall to be a physical defense barrier against pathogen. Upon pathogen infection, plants can promote lignin deposition at infection sites, thereby reinforcing physical barriers to restrict further pathogen spread (Kadota et al. 2015; Tan et al. 2026). In this study, NLR_{4DS-1} apparently promoted secondary metabolic pathways, particularly flavonoid and terpenoid biosynthesis. These metabolites together with lignification form a high-level defense barrier. The biotrophic pathogen *Pst* tends to suppress host cell death and maintain metabolically active "green islands", which are characterized by localized chlorophyll accumulation and sustained nutrient supply (Walters et al. 2008; Kabbage et al. 2017; Thanthrige et al. 2020). However, NLR_{4DS-1} appeared to counteract *Pst*'s strategy by reducing chlorophyll and inducing senescence, which would limit the carbon and energy resources for pathogen growth.

4.3 NLR_{4DS-1} upregulates defensive metabolites, which might provide candidates for green pesticides

Plants often use secondary metabolites as antimicrobial compounds and signaling molecules for defense (Erb and Kliebenstein 2020; Divekar et al. 2022). Flavonoids and terpenoids are important in disease resistance in plants. For example, the SlbHLH95-based flavonoid accumulation enhances tomato resistance to *Botrytis cinerea* (Su et al. 2025); flavonoids and flavonols suppress wheat powdery mildew (Xu et al. 2023). In addition, the terpenoid-based phytoalexins and defense volatiles play roles in rice and tomato immunity (Cao et al. 2022; Lin et al. 2025). However, whether flavonoids and terpenoids enhance *Pst* resistance in wheat remains largely unknown. In this study, the NLR_{4DS-1} transgenic wheat accumulated more flavonoids and terpenoids during a resistant wheat-*Pst* interaction than in the susceptible interaction.

However, the reallocation of carbon skeletons and reducing power to secondary metabolism may affect grain filling or stress tolerance under certain conditions (Zhang et al. 2022; Kumar et al. 2021). In addition, limited metabolites of one or a few types *in planta* may compromise their group effect as for antimicrobial compounds. Currently, the endogenous concentrations of quercetin and borneol in *Pst*-infected wheat leaves remain unknown. If the exogenous level of 100 μM proves to be substantially higher than that attained *in planta*, the observed antifungal effects may largely reflect a pharmacological effect rather than a direct functional role of these metabolites at endogenous levels. Targeted quantification of quercetin and borneol *in planta* will therefore be necessary to determine whether they reach antifungal-effective concentrations in situ, and to fully assess their independent contribution. Thus, it is important to study synergistic interactions among multiple metabolites, as multiple compounds together often exhibit stronger and broader-spectrum antimicrobial activity than a single component. In the future, wheat defense metabolites might be used to develop green pesticides for sustainable agriculture.

5 Conclusion

The *Yr28* gene confers durable *Pst* resistance in *Ae. tauschii*. Here, we prove that the NLR_{4DS-1} alone represents the *Yr28* gene. Multiple transcript isoforms of NLR_{4DS-1} are essential for its full functionality in *Pst* resistance. Mechanistically, NLR_{4DS-1} regulates multiple immune response by: (1) Limiting pathogen nutrient acquisition by preventing a "green island" and causing programmed cell death; (2) Reinforcing physical defenses via lignin deposition; and (3) Activating flavonoid- and terpenoid-based chemical defenses. In the future, the full-length NLR_{4DS-1} will be used to develop durable *Pst* resistance in common wheat.

Supplementary Information The online version contains supplementary material available at https://doi.org/10.1007/s44412-026-00014-w.

Acknowledgements Special thanks to Dr. Lynn Epstein for her critical reading and for editing and polishing the language of this work.

Author contributions D.F. and J.W. conceived the study, secured funding, and revised the manuscript. J. Q. performed most of the experiments and drafted the manuscript. H.K. constructed the PC1334 vector. Z.C.analyzed the transcriptomic data. H. W. characterized transgenic materials, and M. W., F.Y., M. L., and H. T. assisted with the experiments and helped refine the manuscript.

Funding The Key Research and Development Program of the Shandong Province in China, 2024CXPT072-1, and the National Natural Science Foundation of China (32372102).

Data availability All data and findings presented in this study are contained within the article and its supplementary figures and tables.

Declarations

Competing interests The authors declare no competing interests. Author Daolin Fu is the Executive Editor-in-Chief of WheatOmics, Jiajie Wu is a member of the Editorial Board of WheatOmics, and Muhammad Waqas serves as Managing Editor of WheatOmics. These authors were not involved in the editorial handling, peer review process, or decision-making for this manuscript.

Open Access This article is licensed under a Creative Commons Attribution 4.0 International License, which permits use, sharing, adaptation, distribution and reproduction in any medium or format, as long as you give appropriate credit to the original author(s) and the source, provide a link to the Creative Commons licence, and indicate if changes were made. The images or other third party material in this article are included in the article's Creative Commons licence, unless indicated otherwise in a credit line to the material. If material is not included in the article's Creative Commons licence and your intended use is not permitted by statutory regulation or exceeds the permitted use, you will need to obtain permission directly from the copyright holder. To view a copy of this licence, visit http://creativecommons.org/licenses/by/4.0/.

References

Athiyannan N, Zhang P, McIntosh R, Chakraborty S, Hewitt T, Bhatt D, et al. Haplotype variants of the stripe rust resistance gene Yr28 in Aegilops tauschii. Theor Appl Genet. 2022;135:4327–36.

Cao Y, Liu L, Ma K, Wang W, Lv H, Gao M, et al. The jasmonate-induced bHLH gene SlJIG functions in terpene biosynthesis and resistance to insects and fungus. J Integr Plant Biol. 2022;64:1102–15.

Cesari S, Thilliez G, Ribot C, Chalvon V, Michel C, Jauneau A, et al. The rice resistance protein pair RGA4/RGA5 recognizes the Magnaporthe oryzae effectors AVR-Pia and AVR1-CO39 by direct binding. Plant Cell. 2013;25:1463–81.

Chang CY, Yang SX, Zhang MQ, Guo YT, Li XM, Yan Y, et al. Suppression of ZEAXANTHIN EPOXIDASE 1 restricts stripe rust growth in wheat. Plant Commun. 2023;4:100608.

Chen W, Wellings C, Chen X, Kang Z, Liu T. Wheat stripe (yellow) rust caused by Puccinia striiformis f. sp. tritici. Mol Plant Pathol. 2014;15:433–46.

Contreras MP, Pai H, Tumtas Y, Duggan C, Yuen ELH, Cruces AV, et al. Sensor NLR immune proteins activate oligomerization of their NRC helpers in response to plant pathogens. Embo j. 2023;42:e111519.

Deng Y, Zhai K, Xie Z, Yang D, Zhu X, Liu J, et al. Epigenetic regulation of antagonistic receptors confers rice blast resistance with yield balance. Science. 2017;355:962–5.

Denness L, McKenna JF, Segonzac C, Wormit A, Madhou P, Bennett M, et al. Cell wall damage-induced lignin biosynthesis is regulated by a reactive oxygen species- and jasmonic acid-dependent process in Arabidopsis. Plant Physiol. 2011;156:1364–74.

Dibley K, Jost M, McIntosh R, Lagudah E, Zhang P. The wheat stripe rust resistance gene YrNAM is Yr10. Nat Commun. 2024;15:3291.

Divekar PA, Narayana S, Divekar BA, Kumar R, Gadratagi BG, Ray A et al. Plant Secondary Metabolites as Defense Tools against Herbivores for Sustainable Crop Protection. Int J Mol Sci. 2022;23(5):2690.

Erb M, Kliebenstein DJ. Plant Secondary Metabolites as Defenses, Regulators, and Primary Metabolites: The Blurred Functional Trichotomy. Plant Physiol. 2020;184:39–52.

Fu D, Uauy C, Distelfeld A, Blechl A, Epstein L, Chen X, et al. A kinase-START gene confers temperature-dependent resistance to wheat stripe rust. Science. 2009;323:1357–60.

Gou JY, Li K, Wu K, Wang X, Lin H, Cantu D, et al. Wheat Stripe Rust Resistance Protein WKS1 Reduces the Ability of the Thylakoid-Associated Ascorbate Peroxidase to Detoxify Reactive Oxygen Species. Plant Cell. 2015;27:1755–70.

Guo G, Bai K, Hou Y, Gong Z, Zhang H, Wu Q, et al. The wheat NLR pair RXL/Pm5e confers resistance to powdery mildew. Plant Biotechnol J. 2025;23:1260–76.

He Y, Zhang K, Li S, Lu X, Zhao H, Guan C, et al. Multiomics analysis reveals the molecular mechanisms underlying virulence in Rhizoctonia and jasmonic acid-mediated resistance in Tartary buckwheat (Fagopyrum tataricum). Plant Cell. 2023;35:2773–98.

Hovmøller MS, Rodriguez-Algaba J, Thach T, Sørensen CK. Race Typing of Puccinia striiformis on Wheat. Methods Mol Biol. 2017;1659:29–40.

Hu Y, Li M, Li Y, Du L, Xie R, Ni F, et al. A head-to-head NLR gene pair from wild emmer confers stripe rust resistance in wheat. Nat Genet. 2025;57:1543–52.

Huang S, Wang J, Song R, Jia A, Xiao Y, Sun Y, et al. Balanced plant helper NLR activation by a modified host protein complex. Nature. 2025;639:447–55.

Huh SU, Cevik V, Ding P, Duxbury Z, Ma Y, Tomlinson L, et al. Protein-protein interactions in the RPS4/RRS1 immune receptor complex. PLoS Pathog. 2017;13:e1006376.

Ishihama N, Choi SW, Noutoshi Y, Saska I, Asai S, Takizawa K, et al. Oxicam-type non-steroidal anti-inflammatory drugs inhibit NPR1-mediated salicylic acid pathway. Nat Commun. 2021;12:7303.

Janshekar H, Brown C, Fiechter A. Determination of biodegraded lignin by ultraviolet spectrophotometry. Anal Chim Acta. 1981;130:81–91.

Jones JD, Dangl JL. The plant immune system. Nature. 2006;444:323–9.

Kabbage M, Kessens R, Bartholomay LC, Williams B. The Life and Death of a Plant Cell. Annu Rev Plant Biol. 2017;68:375–404.

Kadota Y, Shirasu K, Zipfel C. Regulation of the NADPH Oxidase RBOHD During Plant Immunity. Plant Cell Physiol. 2015;56:1472–80.

Klymiuk V, Yaniv E, Huang L, Raats D, Fatiukha A, Chen S, et al. Cloning of the wheat Yr15 resistance gene sheds light on the plant tandem kinase-pseudokinase family. Nat Commun. 2018;9:3735.

Kong L, Ma X, Zhang C, Kim SI, Li B, Xie Y, et al. Dual phosphorylation of DGK5-mediated PA burst regulates ROS in plant immunity. Cell. 2024;187:609–e623621.

Kong Y, Wang H, Qiao L, Du T, Luo J, Liu Y, et al. Exogenous application of luteolin enhances wheat resistance to Puccinia striiformis f. sp. tritici. Plant Physiol Biochem. 2025;222:109674.

Krattinger SG, Lagudah ES, Spielmeyer W, Singh RP, Huerta-Espino J, McFadden H, et al. A putative ABC transporter confers durable resistance to multiple fungal pathogens in wheat. Science. 2009;323:1360–3.

Kumar V, Thakur JK, Prasad M. Histone acetylation dynamics regulating plant development and stress responses. Cell Mol Life Sci. 2021;78:4467–86.

Lee MH, Jeon HS, Kim SH, Chung JH, Roppolo D, Lee HJ, et al. Lignin-based barrier restricts pathogens to the infection site and confers resistance in plants. Embo j. 2019;38:e101948.

Li W, Wang K, Chern M, Liu Y, Zhu Z, Liu J, et al. Sclerenchyma cell thickening through enhanced lignification induced by OsMYB30 prevents fungal penetration of rice leaves. New Phytol. 2020;226:1850–63.

Lin X, Ding C, Xiao W, Wang J, Lin Z, Sun X, et al. A molecular switch OsWRKY10-OsVQ8 orchestrates rice diterpenoid phytoalexin biosynthesis for broad-spectrum disease resistance. New Phytol. 2025;246:2243–62.

Lyu X, Li G, Su C, Luo X, Zhu Y, Liu T, et al. Current Status and Future Direction of the High-Temperature Resistance in Wheat to Control Stripe Rust. Mol Plant Pathol. 2025;26:e70192.

Mamrutha HM, Sharma D, Sumanth Kumar K, Venkatesh K, Tiwari V, Sharma I. Influence of Diurnal Irradiance Variation on Chlorophyll Values in Wheat: A Comparative Study Using Different Chlorophyll Meters. Natl Acad Sci Lett. 2017;40:221–4.

McNeal F. A Uniform System for Recordin and Processing Cereal Research Data. USDA-ARS; 1971.

Moore JW, Herrera-Foessel S, Lan C, Schnippenkoetter W, Ayliffe M, Huerta-Espino J, et al. A recently evolved hexose transporter variant confers resistance to multiple pathogens in wheat. Nat Genet. 2015;47:1494–8.

Naseem M, Wölfling M, Dandekar T. Cytokinins for immunity beyond growth, galls and green islands. Trends Plant Sci. 2014;19:481–4.

Ngou BPM, Jones JDG, Ding P. Plant immune networks. Trends Plant Sci. 2022;27:255–73.

Ni F, Zheng Y, Liu X, Yu Y, Zhang G, Epstein L, et al. Sequencing trait-associated mutations to clone wheat rust-resistance gene YrNAM. Nat Commun. 2023;14:4353.

Ortiz-Morea FA, Liu J, Shan L, He P. Malectin-like receptor kinases as protector deities in plant immunity. Nat Plants. 2022;8:27–37.

Qian C, Ji Z, Sun Y, Zhang M, Kan J, Xiao L et al. Lignin Biosynthesis in Postharvest Water Bamboo (Zizania latifolia) Shoots during Cold Storage Is Regulated by RBOH-Mediated Reactive Oxygen Species Signaling. J Agric Food Chem. 2023;71(7):3201–3209.

Schmittgen TD, Livak KJ. Analyzing real-time PCR data by the comparative C(T) method. Nat Protoc. 2008;3:1101–8.

Su D, Wu M, Wang H, Shu P, Song H, Deng H, et al. Bi-functional transcription factor SlbHLH95 regulates fruits flavonoid metabolism and grey mould resistance in tomato. Plant Biotechnol J. 2025;23:2083–94.

Takagi H, Uemura A, Yaegashi H, Tamiru M, Abe A, Mitsuoka C, et al. MutMap-Gap: whole-genome resequencing of mutant F2 progeny bulk combined with de novo assembly of gap regions identifies the rice blast resistance gene Pii. New Phytol. 2013;200:276–83.

Tan W, Wang Y, Shang T, Zhu Z, Wang X, Meng S, et al. OsTB1 Coordinately Enhances Rice Culm Strength and Blast Resistance by Promoting Lignin Biosynthesis. Plant Biotechnol J. 2026;24:1652–4.

Thanthrige N, Jain S, Bhowmik SD, Ferguson BJ, Kabbage M, Mundree S, et al. Centrality of BAGs in Plant PCD, Stress Responses, and Host Defense. Trends Plant Sci. 2020;25:1131–40.

Vafaei N, Ribeiro RA, Camarinha-Matos LM. Comparison of Normalization Techniques on Data Sets With Outliers. Int J Decis Support Syst Technol (IJDSST). 2022;14:1–17.

Walters DR, McRoberts N, Fitt BD. Are green islands red herrings? Significance of green islands in plant interactions with pathogens and pests. Biol Rev Camb Philos Soc. 2008;83:79–102.

Wang YD, Liu N, Liu QR, Jiang F. Experimental handbook for plant biology. Beijing: Higher Education Press; 2011.

Wang S, Li QP, Wang J, Yan Y, Zhang GL, Yan Y, et al. YR36/WKS1-Mediated Phosphorylation of PsbO, an Extrinsic Member of Photosystem II, Inhibits Photosynthesis and Confers Stripe Rust Resistance in Wheat. Mol Plant. 2019;12:1639–50.

Wang H, Zou S, Li Y, Lin F, Tang D. An ankyrin-repeat and WRKY-domain-containing immune receptor confers stripe rust resistance in wheat. Nat Commun. 2020;11:1353.

Wang N, Fan X, He M, Hu Z, Tang C, Zhang S, et al. Transcriptional repression of TaNOX10 by TaWRKY19 compromises ROS generation and enhances wheat susceptibility to stripe rust. Plant Cell. 2022;34:1784–803.

Wang L, Xu G, Li L, Ruan M, Bennion A, Wang GL, et al. The OsBDR1-MPK3 module negatively regulates blast resistance by suppressing the jasmonate signaling and terpenoid biosynthesis pathway. Proc Natl Acad Sci U S A. 2023;120:e2211102120.

Wang K, Ren W, Hong L, Wang Q, Ghimire R, Haapanen M, et al. Linalool and 1,8-Cineole as Constitutive Disease-Resistant Factors of Norway Spruce Against Necrotrophic Pathogen Heterobasidion Parviporum. Plant Cell Environ. 2025a;48:1993–2008.

Wang YR, Zhang R, Wang D, Wang Y, Fu ZQ. Activation and suppression mechanisms of the NRG1 helper NLRs. J Integr Plant Biol. 2025b;67(8):1985–1987.

Wu B, Qi F, Liang Y. Fuels for ROS signaling in plant immunity. Trends Plant Sci. 2023;28:1124–31.

Xiao Y, Wu X, Wang Z, Ji K, Zhao Y, Zhang Y, et al. Activation and inhibition mechanisms of a plant helper NLR. Nature. 2025;639:438–46.

Xu W, Xu X, Han R, Wang X, Wang K, Qi G, et al. Integrated transcriptome and metabolome analysis reveals that flavonoids function in wheat resistance to powdery mildew. Front Plant Sci. 2023;14:1125194.

Yan Y, Li XM, Chen Y, Wu TT, Ding CH, Zhang MQ, et al. Phosphorylation of KAT-2B by WKS1/Yr36 redirects the lipid flux to jasmonates to enhance resistance against wheat stripe rust. J Genet Genomics. 2023;50:872–82.

Yan Y, Wang ML, Zhang Z, Liu G, Wei WX, Shi XT, et al. Suppressing wheat sucrose phosphate synthase 1-B protects wheat against stripe rust. J Adv Res. 2025;74:137–51.

Yang Y, Zhao Y, Zhang Y, Niu L, Li W, Lu W, et al. A mitochondrial RNA processing protein mediates plant immunity to a broad spectrum of pathogens by modulating the mitochondrial oxidative burst. Plant Cell. 2022;34:2343–63.

Yang Y, Furzer OJ, Fensterle EP, Lin S, Zheng Z, Kim NH, et al. Paired plant immune CHS3-CSA1 receptor alleles form distinct hetero-oligomeric complexes. Science. 2024;383:eadk3468.

Yuan M, Ngou BPM, Ding P, Xin XF. PTI-ETI crosstalk: an integrative view of plant immunity. Curr Opin Plant Biol. 2021;62:102030.

Zhang C, Huang L, Zhang H, Hao Q, Lyu B, Wang M, et al. An ancestral NB-LRR with duplicated 3'UTRs confers stripe rust resistance in wheat and barley. Nat Commun. 2019;10:4023.

Zhang H, Zhu J, Gong Z, Zhu JK. Abiotic stress responses in plants. Nat Rev Genet. 2022;23:104–19.

Zhang H, Zhang X, Xu M, Yan N, Du Y, Song Z, et al. PuRBOHF-PuPRX42-like complex activates lignin biosynthesis for stone cell formation in pear fruit. Plant Sci. 2025;362:112738.

Zhao S, Ye Z, Stanton R. Misuse of RPKM or TPM normalization when comparing across samples and sequencing protocols. RNA. 2020;26:903–9.

Zhu K, Li M, Dong L, Zhang H, Zhang D, Lu P, et al. An atypical NLR pair TdCNL1/TdCNL5 from wild emmer confers powdery mildew resistance in wheat. Nat Genet. 2025;57:1553–62.

Publisher's note Springer Nature remains neutral with regard to jurisdictional claims in published maps and institutional affiliations.